

Transmission electron microscopy study of plastic deformation in NiZr₂

D. GALY, L. BOULANGER

Section de Recherches de Métallurgie Physique, DTA/CEREM/DTM, C.E. Saclay, 91191 Gif sur Yvette, France

Plastic deformation mechanisms in the body centred tetragonal (C16-structure) NiZr₂ compound have been studied using transmission electron microscopy. Dislocations, stacking faults and microtwins have been characterized. Four families of dislocations have been identified: screw-type ($\mathbf{b}=[001]$), edge-type ($[001](110)$ and $[110](1\bar{1}0)$ systems) and mixed-type ($\frac{1}{2}[1\bar{1}1](110)$ system). Partial dislocations associated with stacking faults have also been detected and analysed. The plane of the faults is shown to be $(1\bar{1}0)$ and the fault vectors $\frac{1}{4}[111]$ and $\frac{1}{4}[11\bar{1}]$. A hard-sphere model illustrating the formation mechanism of these stacking faults is proposed. The microtwins are found to be 60° rotation twins around the $[1\bar{1}0]^*$ direction and can be described by the stacking faults scheme.

1. Introduction

Many intermetallic compounds undergo a crystal-to-amorphous transformation under irradiation [1] or sustained plastic strain, as in mechanical grinding [2].

It is now well established that collapse of the crystalline phase into an amorphous one can be promoted by the accumulation of defects: Frenkel pairs and antisite defects (chemical disorder), dislocations or interstitials [3–6]. Among the mechanisms for producing chemical disorder by mechanical means, one is the nucleation and slip of imperfect dislocations. The stacking faults produced may disorder the crystal on more than one atomic distance. When the dislocation density increases the overlap of disordered regions might induce amorphization.

This work was aimed at examining this hypothesis in the Ni–Zr system which exhibits seven ordered compounds and for which extensive experimental and computer simulation results are available. For example, molecular dynamics simulations made by Massobrio *et al.* [4] demonstrated clearly that amorphization of NiZr₂ can be mediated by chemical disorder (in the form of antisite defects). Experimentally, Chen *et al.* [2] showed that NiZr, NiZr₂ and Ni₁₀Zr₇ amorphize easily on mechanical grinding.

Consequently, we have chosen to study the effects of plastic deformation in Ni_xZr_{1-x} compounds because little information is known about the deformation microstructure. Straining by indentation was chosen, following the work of Clarke *et al.* [7] who found amorphization in silicon and germanium under Vickers indentation. In a previous paper [8], a microstructural analysis of C-base centred orthorhombic NiZr compound deformed at room temperature by Vickers microindentation was performed by transmission electron microscopy (TEM). Several dislocation families and some microtwins have been

characterized but neither imperfect dislocations nor evidence for crystal-to-amorphous transformation were found. In this paper we report TEM analyses of dislocations, stacking faults and microtwins in deformed body centred tetragonal (C16-structure) NiZr₂ compound.

2. Experimental procedure

20 g ingots of 33.33 at % Ni–66.67 at % Zr were prepared by levitation melting of 99.99% Ni and 99.99% Zr under a helium atmosphere. The ingots were annealed under dynamic vacuum at 980 °C for 48 h to reduce internal stresses. After cutting into 500 μm thick slices (by means of an Al₂O₃ saw) and spark-cutting into 3 mm diameter discs, the samples were mechanically ground and polished down to a thickness of ~ 200 μm. They were patterned with arrays of regularly spaced indentations, 11 μm along the diagonal, made at room temperature by means of a diamond-pyramid Vickers microindenter with a 0.28 N load (the Vickers hardness is 4.3 GPa). With the indented surface protected by Lacomit varnish, the deformed samples were back-thinned by using an electropolishing technique with a solution of 70% methanol–20% perchloric acid–10% ethylene glycol at –19 °C and 19 V. The thin foils were examined using a Philips CM20 transmission electron microscope operating at 200 kV and equipped with a tilt-rotation stage.

The Burgers vector of dislocations was determined by applying the usual invisibility criterion

$$\mathbf{gb} = 0 \quad (1a)$$

$$\mathbf{g}(\mathbf{b} \wedge \mathbf{u}) = 0, \quad (1b)$$

where g is the diffraction vector, b the Burgers vector and u the unit vector along the direction of the dislocation line.

The fault vector of stacking faults was obtained by applying the invisibility criterion

$$gR \text{ integral} \quad (2)$$

where R is the fault vector.

Crystals were oriented with the help of stereographic projections.

3. Results and discussion

3.1. Undeformed material

Electron probe analysis of the annealed ingot revealed a slight off-stoichiometric composition. The material consists of NiZr_2 grains more than $100 \mu\text{m}$ in diameter including some small round-shaped zirconium precipitates (a few nanometres in diameter) the proportion of which is below 5 vol %. TEM observations of the NiZr_2 microstructure showed that the grains contain a low dislocation density ($\sim 10^7 \text{ cm}^{-2}$). Those dislocations have been analysed and four families have been identified. Fig. 1a shows screw dislocations of Burgers vector $b = [001]$. For some of them, deviation of the line from the $[001]$ direction resulting from cross-slip is observed. Two families are edge-type and belong to the slip system $[001] (110)$ and $[1\bar{1}0] (110)$ (see Fig. 1b). Lastly some mixed-type dislocations have also been found, they belong to the slip

system $\frac{1}{2}[1\bar{1}1] (110)$. Burgers vectors $b = [001]$ and $\frac{1}{2}[1\bar{1}1]$ could be expected because they represent the two smallest lattice-translation vectors in the ordered NiZr_2 phase, respectively $[001] = 0.527 \text{ nm}$ followed by $\frac{1}{2}[1\bar{1}1] = 0.529 \text{ nm}$. From those slip system analyses it is clear that (110) is a preferred glide plane in NiZr_2 . This is consistent with previous experimental results of Ignat and Durand [9] who showed that (110) planes are easy glide planes in the isostructural compound CuAl_2 .

3.2. Microstructure of deformed samples

In the deformed state, no amorphous phase is found near or under the indentation. Plastic deformation of NiZr_2 produces microtwins, induces a notable increase of the dislocation density ($\sim 10^{10} \text{ cm}^{-2}$) and produces imperfect dislocations.

3.2.1. Stacking faults

Fig. 2a is a bright-field image showing some imperfect dislocations which are likely to be concentric loops issued from a same source. Stereographic analysis reveals that the stacking faults between those dislocations are lying on the $(1\bar{1}0)$ plane. In Fig. 2b they are seen edge-on. As can be seen in Fig. 2c, there are two different stacking faults (one of them is visible and the other out of contrast). According to the analysis of

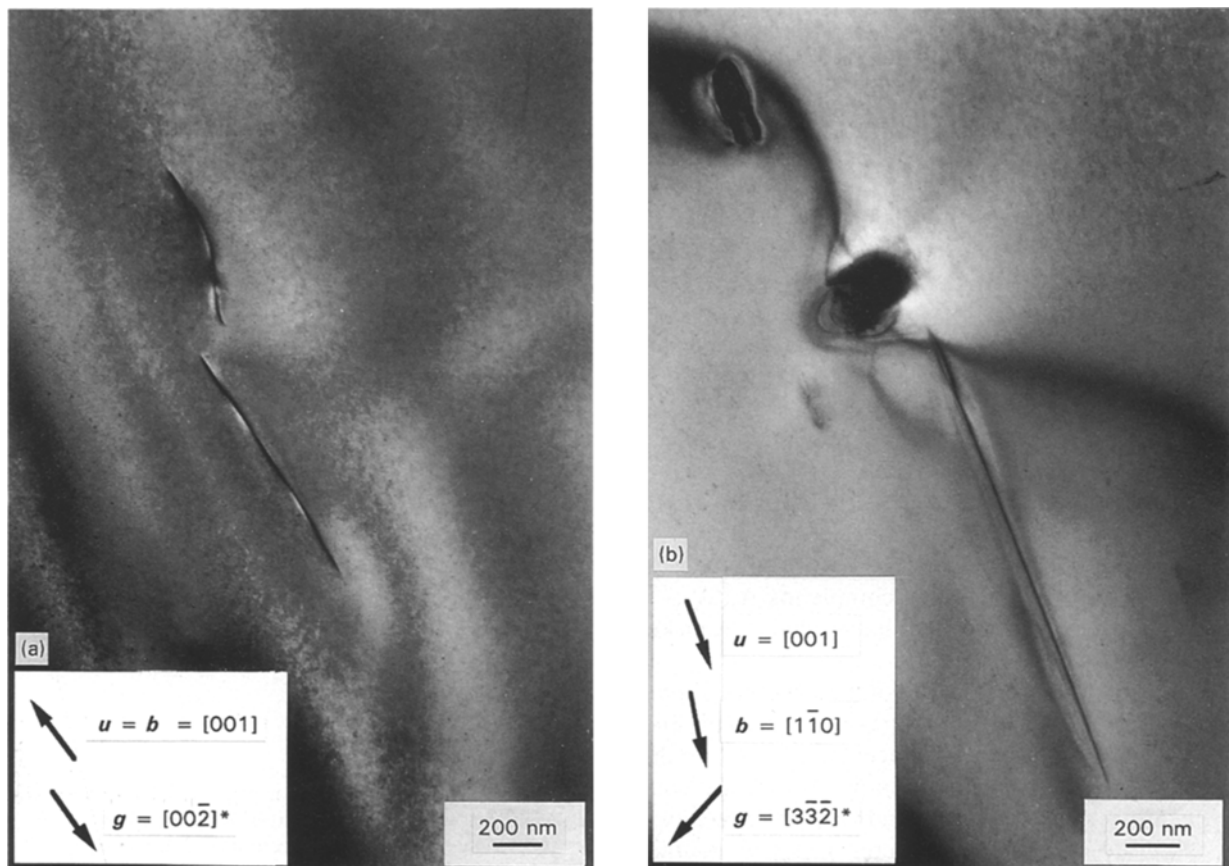


Figure 1 Bright-field images of two families of dislocations: (a) screw dislocations of Burgers vector of $b = [001]$; one of them has cross-slipped, (b) an edge dislocation of slip system $[1\bar{1}0] (110)$; the presence of zirconium precipitates is due to a slight off-stoichiometric composition of the prepared ingots.

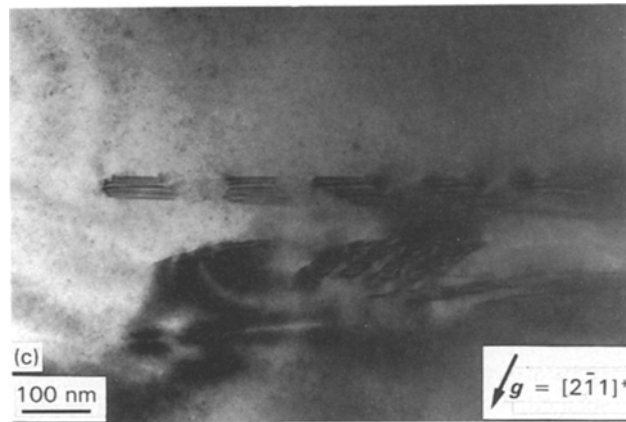
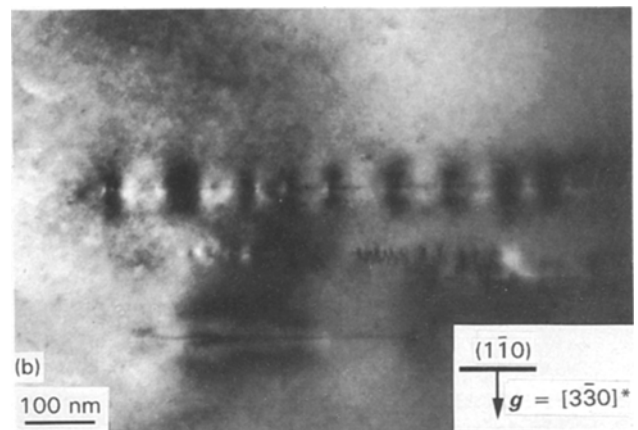
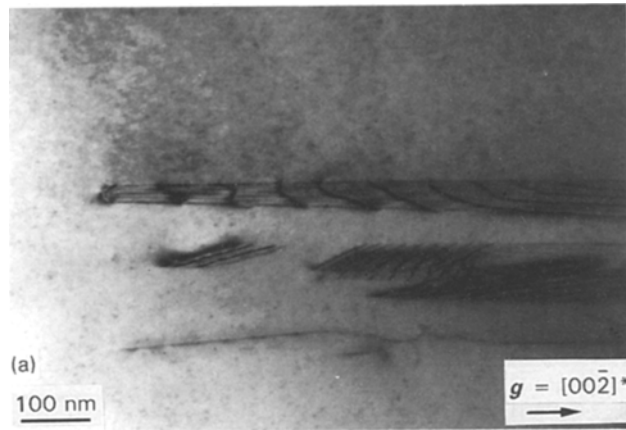


Figure 2 Bright-field images of imperfect dislocations in the same area of a NiZr₂ deformed sample, about 20 μm away from a typical microindentation. Stacking fault between dislocation is of vector $R_1 = \frac{1}{4}[111]$ or $R_2 = \frac{1}{4}[11\bar{1}]$. (a) The two stacking faults R_1 and R_2 are visible; (b) the stacking faults plane is oriented edge-on; (c) fringes due to the R_1 fault are visible; but R_2 is out of contrast because R_2g is integral.

micrographs taken with different diffraction conditions, the displacement vectors are

$$R_1 = \frac{1}{4}[111] \quad (3a)$$

and

$$R_2 = \frac{1}{4}[11\bar{1}]. \quad (3b)$$

The stacking faults scheme has been represented by means of a hard-spheres model. Such a model seems to be valid for NiZr₂ because atomic radius and hard-sphere radius are in the same range ($r_{HS\ Zr} \sim 0.152$ compared with $r_{at} \sim 0.159$ nm and $r_{HS\ Ni} \sim 0.122$ compared with $r_{at} \sim 0.125$ nm). The structure of NiZr₂ can be viewed as a stacking of eight layers parallel to (1 $\bar{1}$ 0): A₁B₁CB₂A₂B₂CB₁. However, as layers A correspond to mirror planes, five layers are enough to describe the structure (A₁B₁CB₂A₂):

at $z = \pm 0.229$ nm, layers A₁/A₂ are pure zirconium with honeycomb structure,

at $z = \pm 0.076$ nm, layers B₁/B₂ are low-density hexagonal layers of zirconium completing A₁/A₂,

at $z = 0$, layer C consists of linear chains in nickel parallel to [001].

Fig. 3 visualizes this analysis of the structure. Zirconium atoms in A-type layer form a honeycomb and the zirconium atoms in the adjacent layer B fill up the empty centres of the hexagons in the A layer. Because of the mirror symmetry, A is sandwiched between two identical layers B, the B spheres being in contact across the A layer. Owing to this arrangement, layers A are "passive" layers under shear and a shift of layer B with respect to layer A seems to be difficult in the (1 $\bar{1}$ 0) plane. In fact, the stacking faults involve only

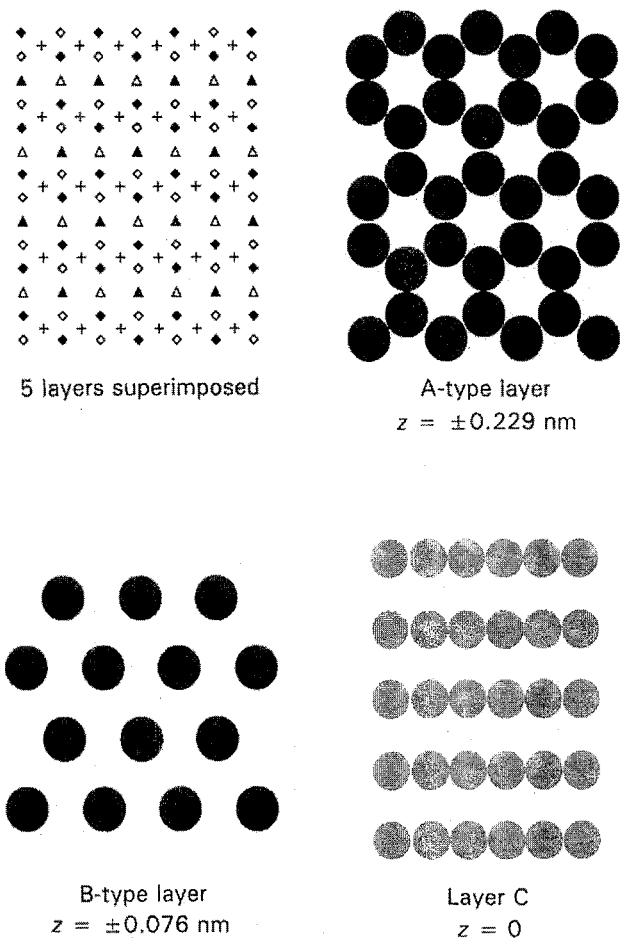


Figure 3 Atom planes stacking geometry in (1 $\bar{1}$ 0) plane. The stacking sequence is A₁B₁CB₂A₂ with layers A mirrors: layers A₁ and A₂ (◇, ◊ at $z = \pm 0.229$ nm) are constituted of zirconium atoms and have a honeycomb structure; layers B₁ and B₂ (△, ▲ at $z = \pm 0.076$ nm) are also constituted of zirconium atoms and complete the A₁ and A₂ honeycombs, respectively; layer C (+ at $z = 0$) is constituted by nickel atoms and consists of columns parallel to the [001] direction.

layers B and C. Nickel atoms of layer C (between B_1 and B_2) must be considered as sitting on two sublattices C_1 and C_2 , where C_1 is fixed with respect to B_1 , and C_2 is fixed with respect to B_2 . The corrugated plane ($B_2 + C_2$) glides over the corrugated plane ($B_1 + C_1$) along $R_1 = \frac{1}{4}[111]$ or $R_2 = \frac{1}{4}[11\bar{1}]$ as shown (for R_2) in Fig. 4. The only difference between the final configuration and the initial one is in the direction of the linear chains of nickel atoms (parallel to rough chains of zirconium formed by layers B_1 and B_2) which have undergone a 60° rotation in the $(1\bar{1}0)$ plane. The stacking fault conserves the surroundings of every atom.

Unfortunately, the partial dislocations bordering the stacking faults could not be analysed because of the strong contrast of stacking fault fringes and a large thickness in available areas.

3.2.2. Twinning

Fig. 5a shows a typical microstructure about $5\ \mu\text{m}$ away from a microindentation. The structure consists of a high concentration of deformation microtwins. They have a thickness of about 2 nm (see Fig. 5b) and the twin plane is $(1\bar{1}0)$. The formation mechanism of these twins can be understood from the above description of stacking faults. Indeed stacking faults lying in the $(1\bar{1}0)$ plane with displacement vectors $R = \frac{1}{4}[111]$ or $\frac{1}{4}[11\bar{1}]$ and are obtained by gliding of layer B_1 over B_2 (and vice versa). A succession of such stacking faults R introduced between the B_1 and B_2

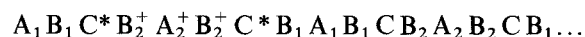
layers (starting from the twin plane) produces in elementary structures a translation proportional to the distance from the twin plane. As can be seen in Fig. 4 illustrating the fault scheme, the glide of $R = \frac{1}{4}[11\bar{1}]$ produces on sequence $A_1B_1CB_2A_2$ a new arrangement which would be obtained by a $+60^\circ$ rotation around $[1\bar{1}0]^*$. The stacking fault applied on



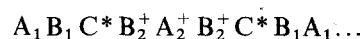
to the first sequence "BCB" gives



where C^* is the configuration obtained from layer C by a 60° rotation around $[1\bar{1}0]^*$ and X^+ is obtained from X by a translation of vector R . The second stacking fault applied to the second sequence "BCB" gives



since $2R$ is a lattice-translation vector. Finally, applying an n th stacking fault to the n th sequence "BCB" gives the twin sequence



or

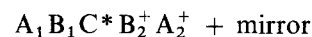


Fig. 6 shows (for $R = \frac{1}{4}[11\bar{1}]$) this geometry relative to layers B and C (layers A can be deduced of their adjacent layer B). They are 60° rotation twins: the orientation of the twin-crystal can be deduced from the initial one by a 60° rotation around the $[1\bar{1}0]^*$ direction. Similarly a succession of $R = \frac{1}{4}[111]$

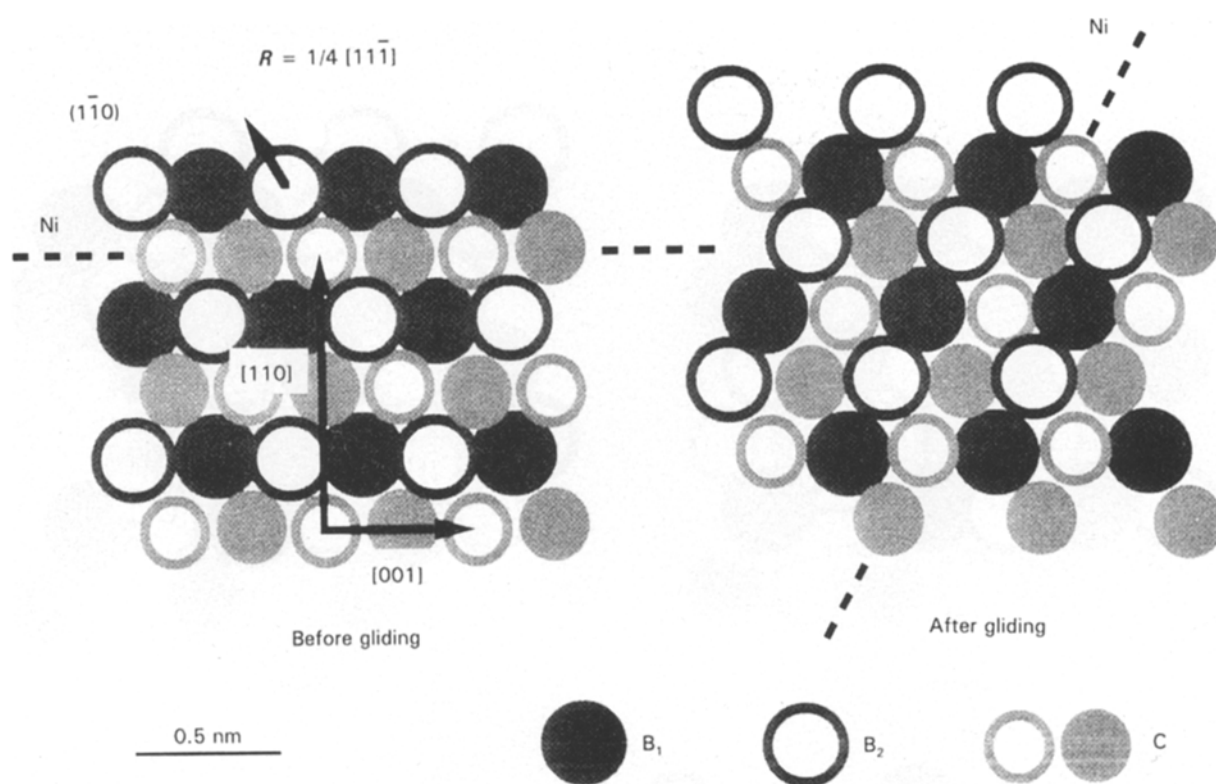


Figure 4 Schematic illustration of the $R_2 = \frac{1}{4}[11\bar{1}]$ stacking fault in the $(1\bar{1}0)$ plane using only sequence B_1CB_2 . Dark-grey filled discs correspond to atom layer B_1 at $z = -0.076\ \text{nm}$, dark-grey opened discs to layer B_2 at $z = +0.076\ \text{nm}$. At $z = 0$, nickel atoms of layer C must be considered in two sublattices (C_1 : filled atoms and C_2 : opened atoms). The stacking fault is performed by the gliding on layer B_1 of layer B_2 driving C_2 . Note the new orientation of nickel chains after gliding (see text).

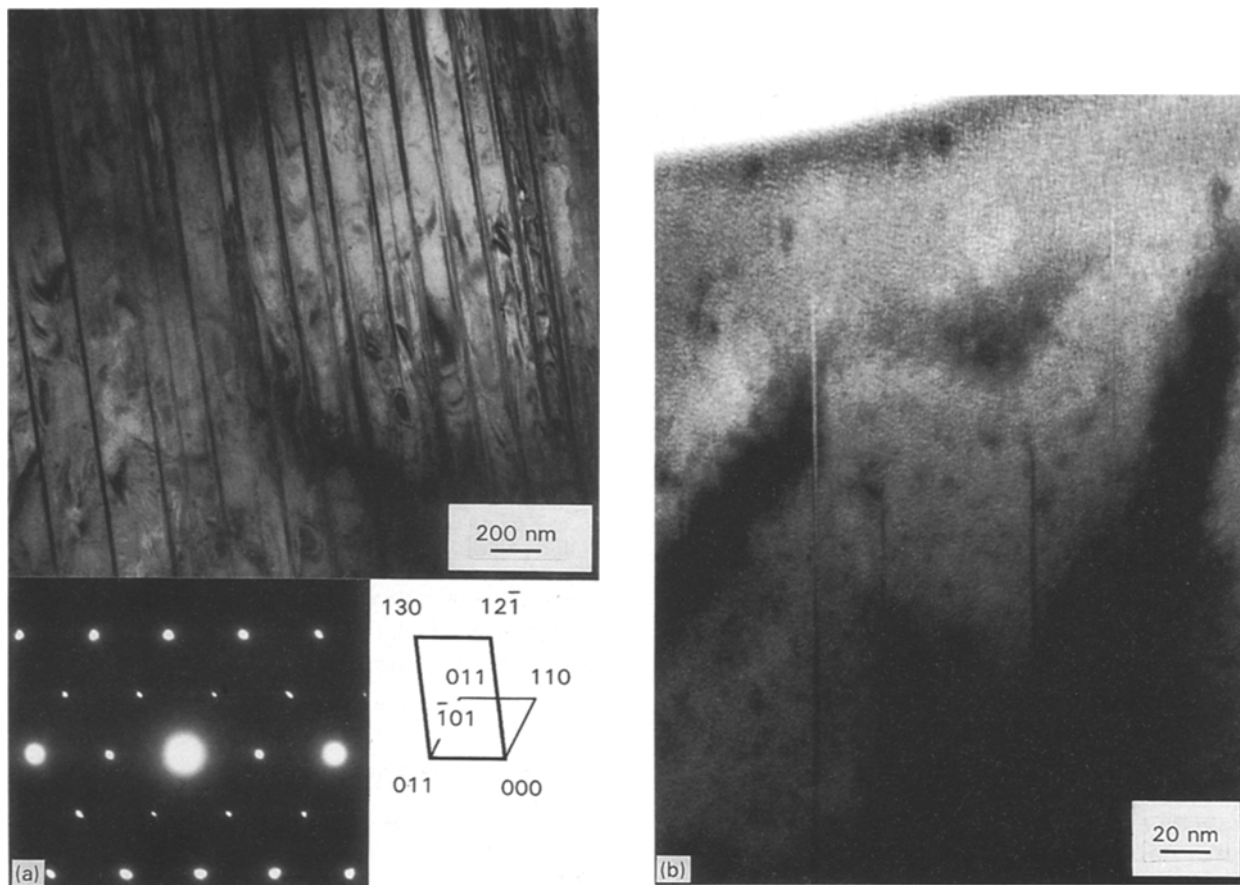


Figure 5 Transmission electron micrographs of a region 5 μm away from a microindentation. (a) Note the high density of microtwins lying on $(1\bar{1}0)$ planes; dislocations between the twins belong to the slip system of $[001](110)$. The diffraction pattern of this region consists of high-intensity spots relating to the matrix, and weaker intensity spots relating to the microtwins. Indexation of such a diffraction pattern confirms the assumption of a 60° rotation around $[1\bar{1}0]^*$ twinning. (b) Microtwins of a few nanometres thickness are seen twin plane edge-on.

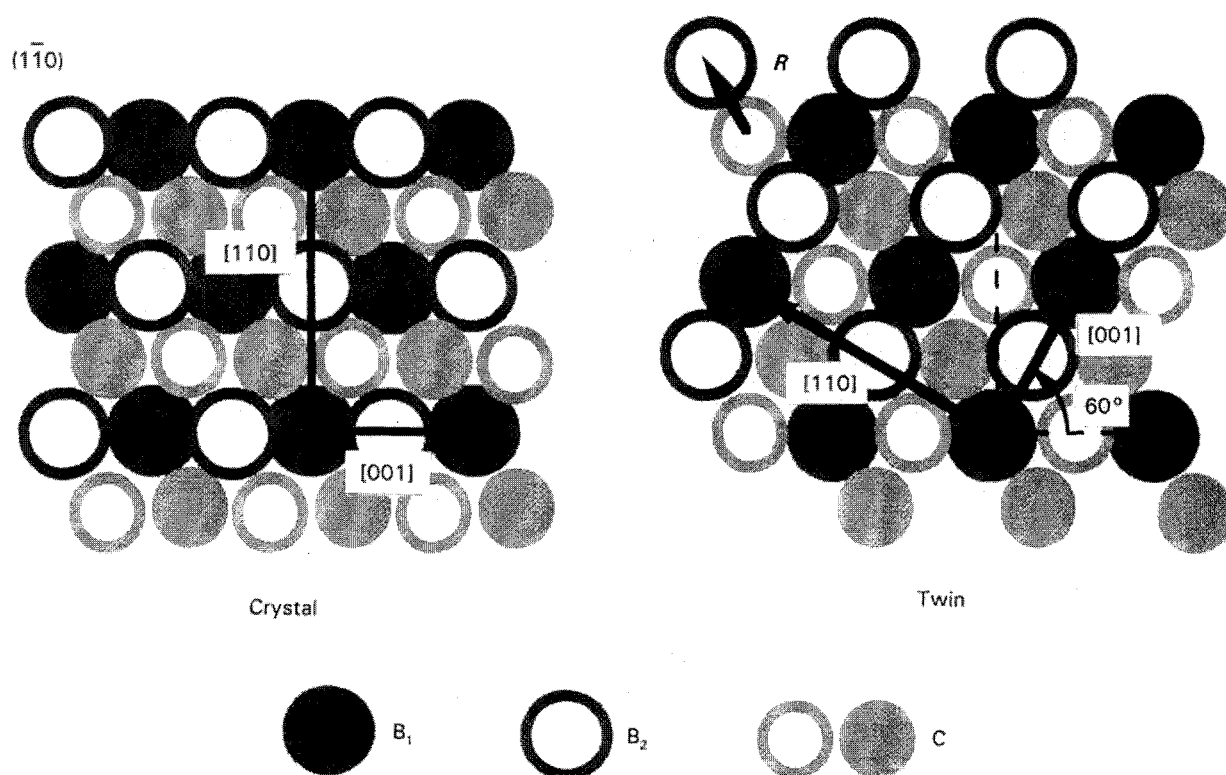


Figure 6 Schematic illustration of the 60° rotation (around $[1\bar{1}0]^*$) twinning in NiZr_2 produced by a succession of stacking faults of fault vector $R_2 = \frac{1}{4}[1\bar{1}\bar{1}]$. Similarly, the $R_1 = \frac{1}{4}[111]$ fault produces a -60° rotation twin.

produces a -60° rotation twin around the $[1\bar{1}0]^*$ direction. This theoretical model has been confirmed with the help of the TEM analyses. Thus selected-area diffraction patterns from microtwins and matrix have been indexed (see also Fig. 5a).

4. Conclusion

Indentation of NiZr_2 creates microtwins, perfect and partial dislocations. Stacking faults and twins have been identified and characterized. Analysis of areas under the indentation has revealed no evidence for crystal-to-amorphous transformation. Such stress accommodation mechanisms prevent the compound from amorphizing under indentation.

Acknowledgements

We thank Professor J. P. Poirier and Dr G. Martin for fruitful discussions and critical reading of the manuscript.

References

1. H. MORI, H. FUJITA, M. TENDO and M. FUJITA, *Scripta Metall.* **18** (1984) 783.
2. Y. CHEN, R. LE HAZIF and G. MARTIN, *Solid State Phenom.* **23-24** (1992) 271.
3. Y. LIMOGÉ, A. RAHMAN, S. HSIEH and S. YIP, *J. Non-Cryst. Solids* **99** (1988) 75.
4. C. MASSOBRIO, V. PONTIKIS and G. MARTIN, *Phys. Rev. B.* **45** (1991) 2484.
5. H. BAKKER, L. M. DI and D. M. L. R. CASCIO, in "Proceedings of the international symposium on mechanical alloying", Kyoto, Japan, Materials Science Forum Vols **88-90** edited by P. H. Shingu (Trans. Tech Publications, Switzerland, 1992) p. 27.
6. M. J. SABOCHICK and N. Q. LAM, *Phys. Rev. B* **43** (1991) 5243.
7. D. R. CLARKE, M. C. KROLL, P. D. KIRCHNER and R. F. COOK, *Phys. Rev. Lett.* **60** (1988) 2156.
8. D. GALY and L. BOULANGER, *Phys. Stat. Sol.* **a139** (1992) K81.
9. M. IGNAT and F. DURAND, *Scripta Metall.* **10** (1976) 623.

Received 7 January

and accepted 21 September 1994